Synchronous and Asynchronous Integrations in an Ocean General Circulation Model

YONGFU XU

Kansai Environmental Engineering Center Co., Chuo-ku, Osaka, Japan

SHIGEAKI AOKI AND KOH HARADA

National Institute for Resources and Environment, Tsukuba, Ibaraki, Japan

(Manuscript received 30 October 2000, in final form 2 April 2001)

ABSTRACT

A basinwide ocean general circulation model of the North Pacific is used to study the difference in distributions of tracers between asynchronous and synchronous integrations. An integration in which equal time steps and no depth acceleration are applied is called a synchronous integration. On the contrary, the integration is called asynchronous integration or acceleration. The acceleration can be divided into tracer acceleration and depth acceleration. Only the tracer acceleration is examined in this study. The values of 48, 24, 12, 6, 3, and 1 for the ratio (α) of tracer time step to momentum time step are used in the model. Results show that a 15-yr integration adjustment is necessary for tracers to reach a new state at which there is a 1% difference from a final state upon a switch to a smaller tracer time step from an equilibrium state. The too large ratio of 48 generally produces an unacceptable departure from synchronous integration. If a difference of about 3% is allowed, the ratio of about 8 can be used. The largest difference mainly appears at the subsurface of the Tropics. This is mainly due to destruction of geostrophic balance at the equator. Clorofluorocarbons (CFCs) are taken as a reference to study the distribution of passive or anthropogenic tracers using different α values. The results from several 10-yr runs show that the largest α value of 48 generates an over 10% error in distributions of CFC-11, compared with the case of $\alpha = 1$. Decreases in α values reduce the error. When α is less than 12, an asynchronous integration of the CFC model will not generate an over 3% error in CFC distributions.

1. Introduction

Since the ocean takes many thousands of years to spin up, it is computationally hard to use synchronous integration from the onset. The numerical acceleration methods are often used to speed up the convergence of the equilibrium solution. The acceleration technique has been widely used in the ocean modeling work, which was elucidated by Bryan (1984). We can consider the acceleration as tracer acceleration and depth acceleration. So-called tracer acceleration indicates that the time step for tracers is larger than that for the velocity. The depth acceleration means that the time step for tracers (or velocity) in deep water is larger than that in the upper layer. Both depth and trace accelerations are called asynchronous integration.

Bryan (1984) pointed out that asynchronous integration did not affect the final equilibrium solutions under the steady forcing conditions. Annual mean forcing is a representative of this kind of modeling work in order to derive mean circulation features. Weaver and Sarachik (1991) found that the steady state obtained under restoring boundary conditions only changed slightly upon a switch to synchronous integration. However, the acceleration technique should be used carefully in the seasonally forced models as the distorted physics cannot be removed (Bryan 1984). Bryan and Lewis (1979) used a tracer (temperature and salinity) time step that was 23.4 and 10.9 times longer than a velocity time step in the coarse- and high-resolution versions of their global seasonally forced model, respectively. In the basinwide model, Sarmiento (1986) used a tracer time step that was 6 times longer than a momentum time step. Recently Danabasoglu et al. (1996) investigated the equilibrium attained with the acceleration technique, discussed the adjustment from asynchronous integration to synchronous integration, and made some important and useful suggestions. From their comprehensive analysis, we found that the difference of equilibrium attained with between asynchronous and synchronous integrations is not large. Although their synchronous integration was initiated from the results obtained with the accelerated technique, the conclusion would probably not be changed. Some results about seasonal cycles and synchronous adjustments are quite interesting. We see from their comparison of the accelerated and synchronous

Corresponding author address: Dr. Yongfu Xu, Institute of Atmospheric Physics, Chinese Academy of Sciences, Beijing 100029, China.
E-mail: xyf@mail.iap.ac.cn

seasonal cycles for some transports that the change in accelerated amplitudes is slightly smaller (about 10%) but the phase lags from 15 days to 1.5 months. They also pointed out that the accelerated and synchronous seasonal cycles for temperature and salinity near the surface had no major phase and amplitude differences, and that in the middepth and abyssal ocean the adjustment of tracer seasonal cycles due to depth acceleration could be nearly completed within 1 yr of synchronous integration. However, Danabasoglu et al. have not clearly compared the difference of tracer distributions between asynchronous and synchronous integrations. They have not studied the influence of α values on the simulated results either. We are interested in whether or not tracer distributions will be significantly affected by the distorted physics during the integration. We attempt to find out a suitable value for the ratio (α) of the tracer time step to the momentum time step in order to save computer resources. In other words, we try to use an asynchronous integration that does not generate a significant difference relative to synchronous integration. We are particularly interested in the difference of distributions of anthropogenic tracers between asynchronous and synchronous integrations. Our test case showed that there might be some significant differences of tracer distributions in the ocean between the asynchronous and synchronous integrations. The difference depends on the ratio (α) of tracer time step to momentum time step, and can be removed with the adjustment of synchronous integration.

Passive tracers are often used to assess the performance of an ocean general circulation model (OGCM) that is also used to study the cycles of some biogeochemical elements in the ocean. In general, the model of passive tracers is run together with an OGCM in the seasonally forced model after the OGCM reaches an equilibrium cycle. It seems that the synchronous adjustment method (Danabasoglu et al. 1996) is still hard to be applied into models that require the longer integration, such as for the carbon cycle. The availability of computer resources often limits the use of the long-term synchronous integration. Therefore, some researchers still use the different ways to adapt the computer conditions. Probably the difference due to the accelerated technique is negligible, compared with the difference between the current model and the observations. If we are much more interested in the mean features of distributions of tracers in the ocean and allow some small errors, we may not really need to use the strictly synchronous integration or even synchronous adjustment. Nevertheless, an offline tracer model (Follows and Marshall 1996) can also be used to save the computer resources in some applications of OGCMs.

Recently, several studies have been made of oceanic uptakes of some anthropogenic tracers. Craig et al. (1998) used a restoring way for the first 22 yr to speed up the convergence of realistic initial model state for the later chlorofluorocarbon (CFC) simulation. Duffy et al. (1997) conducted the final 25 yr of integration adjustment without depth acceleration after the model reached the equilibrium in terms of depth acceleration in their study of oceanic uptake of natural carbon-14. England and Hirst (1997) used the time step of 1 day for tracers without depth acceleration to study the CFC distribution in their global seasonally forced model.

We are curious about whether or not there is a significant difference of tracer distributions between the synchronous and asynchronous integrations, and about the involved physics. Our model is a basinwide one. Several numerical experiments were conducted, which are described in section 2. A comparison of results is given in section 3. Finally concluding remarks are presented in section 4.

2. Model description and numerical experiments

The OGCM of the North Pacific used in this work was originally developed by Ishida et al. (1995) on the basis of the Geophysical Fluid Dynamics Laboratory model (Bryan 1969). Nevertheless, a large modification has been made, including domain, vertical resolution, and implementation of the mixing scheme of tracers by Gent and McWilliams (1990) and Gent et al. (1995). A basic model configuration has been described in Xu et al. (1999), so a summary is given here. The model domain is the Pacific Ocean north of 20°S. A horizontal resolution is 2° lon × 2° lat. There are 28 vertical levels. The first top level is 50 m, and the maximum model depth is 5750 m. An artificial rigid boundary is set on the southern boundary at 20°S. In all experiments, the vertical diffusivity is 0.3 $cm^2\ s^{-1}$, and the horizontal and vertical viscosities are 1×10^9 and 10 $cm^2\ s^{-1}$, respectively. Isopycnal diffusivity is 2×10^7 $cm^2\ s^{-1}$. The thickness diffusivity is the same as isopycnal diffusivity.

Surface fluxes of momentum are prescribed, and are obtained by linearly interpolating monthly mean wind stresses of Hellerman and Rosenstein (1983) spatially onto the model grid, and temporally into each model day. Surface fluxes of heat and salinity are calculated by restoring model-predicted temperature and salinity in the first level to the observed values derived from the monthly mean observed values (Levitus and Boyer 1994; Levitus et al. 1994, hereafter referred to as the Levitus data) with a timescale of 30 days. The temperature and salinity near the southern boundary (from 20° to 14°S) are also restored to the observed in order to represent the supply of the deep water out of the South Pacific. The restoring timescale along the southern boundary smoothly increases from 60 days at 19°S to infinity at 14°S.

No depth acceleration is used in the model. The model calendar and the forcing fields are based on the tracer time step. The momentum time step is always 30 min, but the tracer time step is different for different cases. Therefore, the annual cycles of heat and salt forcings

are properly applied to the model but the surface wind forcing is not properly applied to the model if α is not equal to 1. Following the way of Danabasoglu et al. (1996), we used two integration phases. During the first phase, the model was integrated for 500 yr using a large time step of 1 day for the tracers to speed up the convergence to equilibrium, which is called case GM0. The spinup was initiated with the ocean at rest and with the temperature and salinity set to their annual mean Levitus values. During the second phase, we used different values for α and restarted the integration with GM0 results as initial conditions for another 50 yr. The numerical experiments of different values of 48, 24, 12, 6, 3, and 1 for α are called GM1, GM2, GM3, GM4, GM5, and GMS. Actually the GM1 is the continuous integration of GM0. The GMS is also called synchronous integration (synchronous adjustment) because the tracer time step is equal to the velocity time step.

In order to understand the difference of simulated distributions of passive tracers caused by asynchronous integration, we restarted model integrations from the results at the end of the above second-phase integrations of OGCM, and included additional passive tracers of CFCs. We intended to evaluate the difference of simulated CFC distributions between the synchronous and asynchronous integrations. Thus, we ran the model only for 10 yr. Atmospheric CFC concentrations from 1980 to 1990 (Bullister and Weiss 1988; Elkins et al. 1993) are used in the model. A formula used for the calculation of CFC flux is the product of the gas transfer velocity and the difference of CFC concentrations between the atmosphere and the ocean. The equation for transfer velocity is the one by Wanninkhof (1992), in which transfer velocity for a given gas is a function of the climatological wind speed and the Schmidt number. Here the annual mean wind speed (Esbensen and Kushnir 1981) is interpolated onto the model grid. CFC solubilities are calculated from the function of temperature and salinity (Warner and Weiss 1985). Atmospheric CFC concentrations are assumed to be homogeneous due to rapid mixing rates in the lower atmosphere and chemical stability in the troposphere. The initial CFC values in the ocean are set to zero for these runs.

3. Results and discussion

Present OGCMs are able to simulate the main features of the large-scale thermohaline circulation, but the apparent difference between the model and the observations still exists, particularly in the thermocline. Our OGCM has a similar deficiency. The simulated temperature profile is warmer than observed. Although the obviously sharp gradient of salinity in the thermocline can be seen in the simulated profile, it is smaller than that in the observations. The differences of potential temperature (hereafter temperature) and salinity between the observations and simulated results are quite small in the deep water.

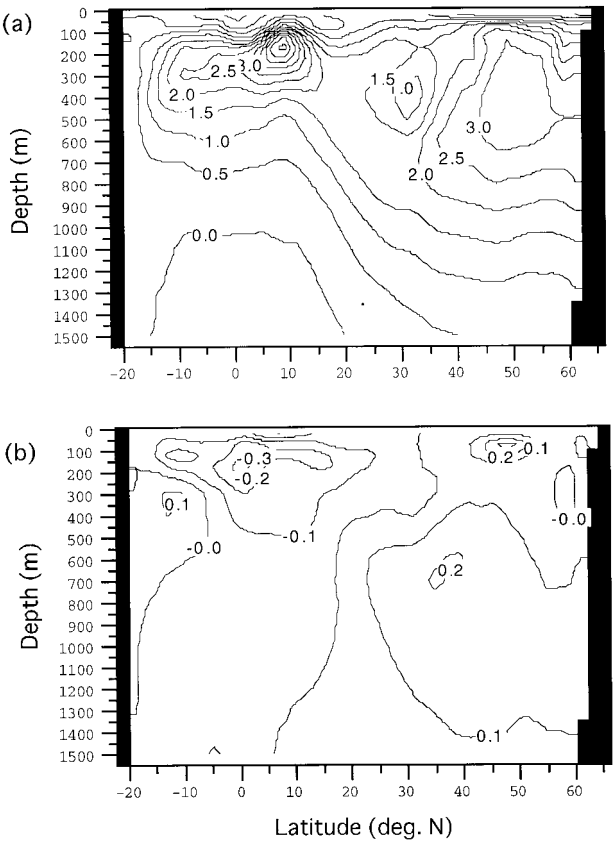

FIG. 1. Differences of zonally averaged annual mean (a) potential temperature and (b) salinity between the model and observations (GMS − LEV). Observed data are from the long-term observed mean from Levitus et al. (1994) and Levitus and Boyer (1994), and the model data are results from the 50th year of GMS simulation. Contour intervals are (a) 0.5°C and (b) 0.1.

Because the seasonal thermohaline variation does not affect the deep water significantly and the main difference between the model and the observation is in the thermocline, next we present the comparison of results at above 1500 or 1000 m. We show in Fig. 1 the difference between simulated results from the last year of synchronous adjustment (GMS) and the zonally averaged annual mean observations (LEV), expressed as GMS − LEV. The model shows a too warm thermocline (Fig. 1a). The largest difference appears at the subsurface at the Tropics, and the next largest difference occurs in higher latitudes with a large area extending into whole thermocline. This is quite common for current OGCMs. At the location of the tongue of observed low-salinity water (North Pacific Intermediate Water) at about 650 m between 30° and 40°N, the model reproduces this main feature in the North Pacific but it has a slightly salty value of over 0.1 (here units of salinity are reported on the dimensionless practical salinity scale). The subsurface is too fresh by up to 0.3 at the Tropics, but too salty by up to 0.3 at about 45°N.

Before we discuss the influence of α values on the

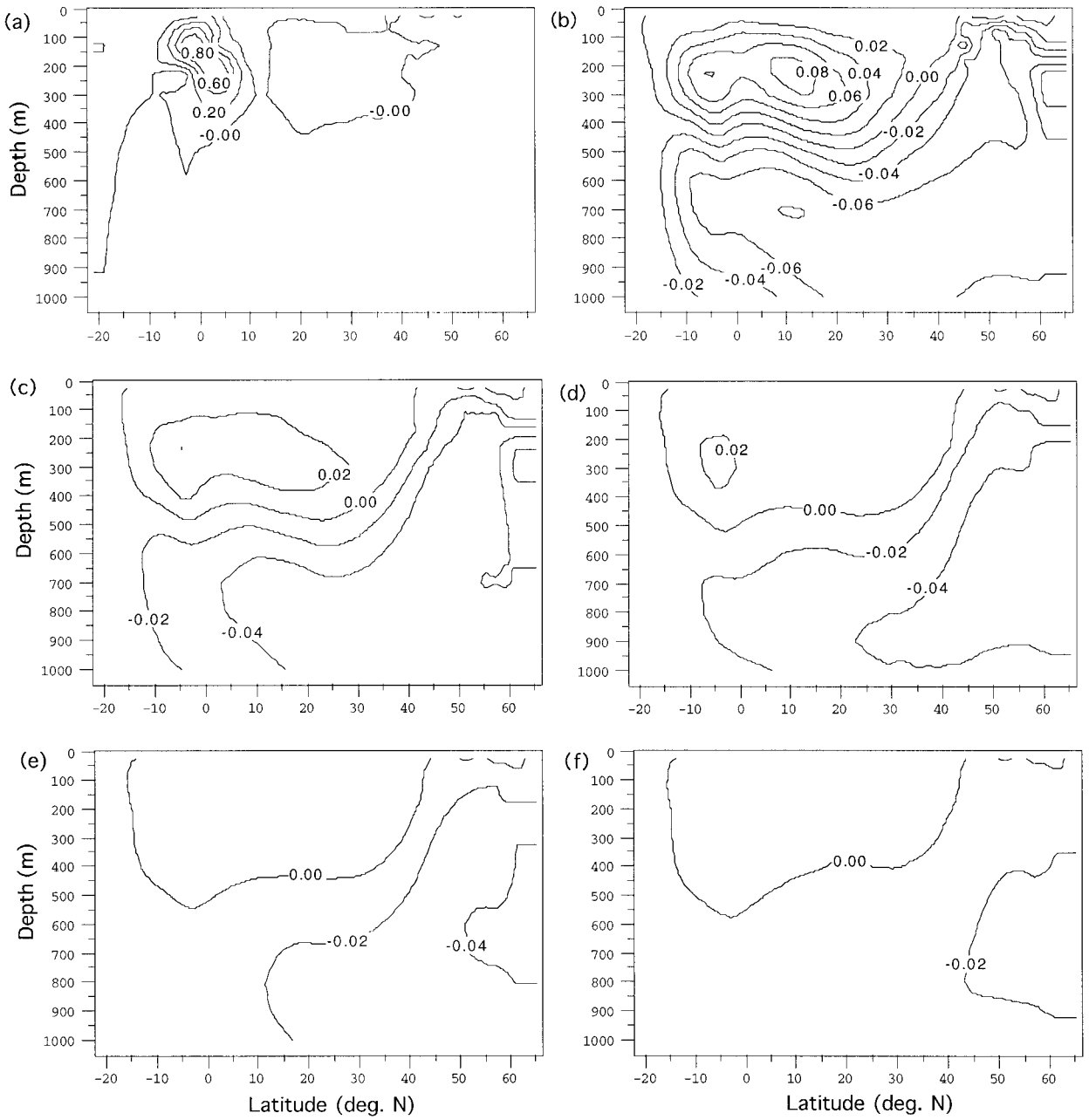

FIG. 2. Evolution of departures of zonally averaged Mar mean temperature from the reference values: (a) GMS(0) − GMS(50), (b) GMS(5) − GMS(50), (c) GMS(10) − GMS(50), (d) GMS(15) − GMS(50), GMS(20) − GMS(50), GMS(30) − GMS(50). GMS(5) indicates the Mar mean temperature of the 5th year of integration. Contour intervals are (a) 0.2°C and (b), (c), (d), (e), and (f) 0.02°C.

simulated results of tracers, we need to know how long the model should be run to make the adjustment of equilibrium state from GM0 to GMn ($n = 1, 2, \ldots$). Danabasoglu et al. (1996) showed that during synchronous adjustment the phase difference disappears almost instantaneously and the full amplitude is recovered after 5 yr. They suggested a 15-yr synchronous adjustment after a sufficient equilibrium state has been achieved with acceleration. We take the results from the last year of GMS integration as a reference to examine the evolution of departures of temperature from it. In fact, we depict differences of the zonally averaged March mean temperature every 5 or 10 yr, which are shown in Fig. 2. For example, GMS(5)–GMS(50) is the difference of March mean temperature between the 5th year and 50th year of integrations. Figure 2a confirms a large difference between accelerated and synchronous integration. At the 5th year, the temperature difference has reduced by about 1 order of magnitude at the upper thermocline, and the larger difference of over 0.1°C at the subsurface

of the Tropics disappears, indicating that the adjustment has completed about 90%. At the 10th year, the difference in the thermocline becomes larger in higher latitudes than at the Tropics. Meanwhile, the lower thermocline is gradually adjusted. After 30 yr, the absolute difference is below 0.02°C except for a small area in higher latitudes. We should point out that a difference of 0.02°C in Fig. 2f is not due to the time trend. The difference between GM0 and the last year of GM1 is generally smaller than 0.002°C except for a very small area near 1000 m in higher latitudes where the difference is about 0.003°C. In the area of above 600 m the difference is less than 0.001°C. There is a time trend of some warming and cooling at the end of the first integration phase (500 yr), which is very normal. Volume-averaged change rates are less than 5×10^{-3} °C century^{-1} for temperature and 6×10^{-4} century^{-1} for salinity, which we considered a steady state. The lower thermocline and deep water still have some warming or cooling trend after 550 yr of integration. It can follow from Fig. 2 that after 15 yr of synchronous adjustment from the accelerated integration, there is still a relative difference of less than 1% in temperature at some areas of thermocline, whereas after 30 yr, the difference becomes less than 0.5%, which should be tolerable in the current OGCM modeling work. Different seasons may have slightly different results. We find that the difference in September is much smaller than that in March. In general, the winter season has a larger difference. These results demonstrate that the synchronous adjustment for tracers is also necessary.

Now we discuss how α values affect the distributions of temperature and salinity. We still take the results from the last year of GMS as a reference. Because there is a phase difference in currents, the difference caused by different α values varies with season. The results shown in Fig. 3 are the differences of zonally averaged March mean temperature relative to GMS from the last year of integrations, expressed as GMn $-$ GMS. Obviously the difference decreases with the decrease in α. The largest difference in Fig. 3a is over 1.0°C, but it reduces to about half of that value in Fig. 3b. The difference between Figs. 3a and 3e is nearly 1 order of magnitude. Similarly, we also find that this kind of difference in wintertime is larger than that in summertime. However, the largest difference appears at the different area. For example, the largest difference in September appears at the subsurface at around 10°N, close to the position of annual mean results (Fig. 1a). The different position of the largest difference is probably related to the phase difference of currents. This is probably associated with the strong wind in wintertime. Figure 4 shows the results of salinity difference in March from different cases. As in Fig. 3, the difference decreases with the decrease in α. The largest difference in Fig. 4a is over 0.1, but it reduces to 0.03 in Fig. 4b. The difference between Figs. 4a and 4e is about 1 order of magnitude. The differences in September are much smaller than those in March.

From Figs. 3 and 4, we can see that if α is 12, the largest relative difference in temperature due to asynchronous integration is over 1%, but for salinity it is less than 0.1%. If α is 6, for temperature it becomes less than 1%, while for salinity less than 0.03%. When α is less than 6, the differences are very small, which can be ignored. To estimate the α value, the volume-averaged absolute temperature differences between accelerated and synchronous integrations are calculated according to the following relation:

$$X = \sum |\Delta T| \Delta V / V,$$

where ΔT represents the temperature difference between GMn and GMS in a grid cell, ΔV is a grid cell volume, and V is model ocean volume. If the March mean values obtained from the final year of integration are used for the calculation, the results of X for $\alpha = 48, 24, 12, 6, 3$ are 0.0396, 0.0334, 0.0274, 0.0176, 0.00869, respectively. The largest X is quite small, which is about 1% of the model domain–averaged temperature value (about 4°C). Here X does not vary linearly with α. When α reduces from 48 to 6, X is roughly only halved, but from 6 to 3 it is also halved.

In addition, we also find out the number of the grid cells with the larger difference. Here we look for the number of grids with $|\Delta T|$ over 1.0° and 0.5°C for simulated March mean temperature. The grid number with $|\Delta T| \geq 1$ is 284, 35, 25, 0, 0, and with $|\Delta T| \geq 0.5$ is 1313, 687, 581, 128, 0, for 5 different α values, respectively. It should be pointed out that all grid cells with larger differences are located at depths less than 500 m. When α is equal to 6, there is no grid cell with the difference of over 1°C, but there are over 100 grids that have the difference of over 0.5°C. We know from Fig. 1a that temperature differences of about 5°C between the simulated and observations in some areas exist in the current models. There are only about 10 grids that have a relative difference of over 2% in annual mean temperature. We believe that using α of 6 will not make any large difference of tracers between the synchronous and asynchronous integrations. When α is equal to 12, there are 25 grids that have the difference of over 1.0°C for March mean temperature. There are about 10 grids that have a relative difference of over 5% in annual mean temperature. If we allow for a slightly larger error of 3%, we can use a value of 8 for α in the OGCMs. With this choice, we can save computer time, but do not significantly change the results of tracer distributions in the ocean.

What causes the difference between asynchronous and synchronous integrations? From Figs. 3 and 4, we see that the main difference from the asynchronous integration appears at the subsurface of the Tropics, which can be clearly seen in Fig. 5. The large time step for the tracer is based on the fact that the timescale for the adjustment of density is much greater than that of velocity. During the asynchronous integration, the velocities come into geostrophic adjustment with the density.

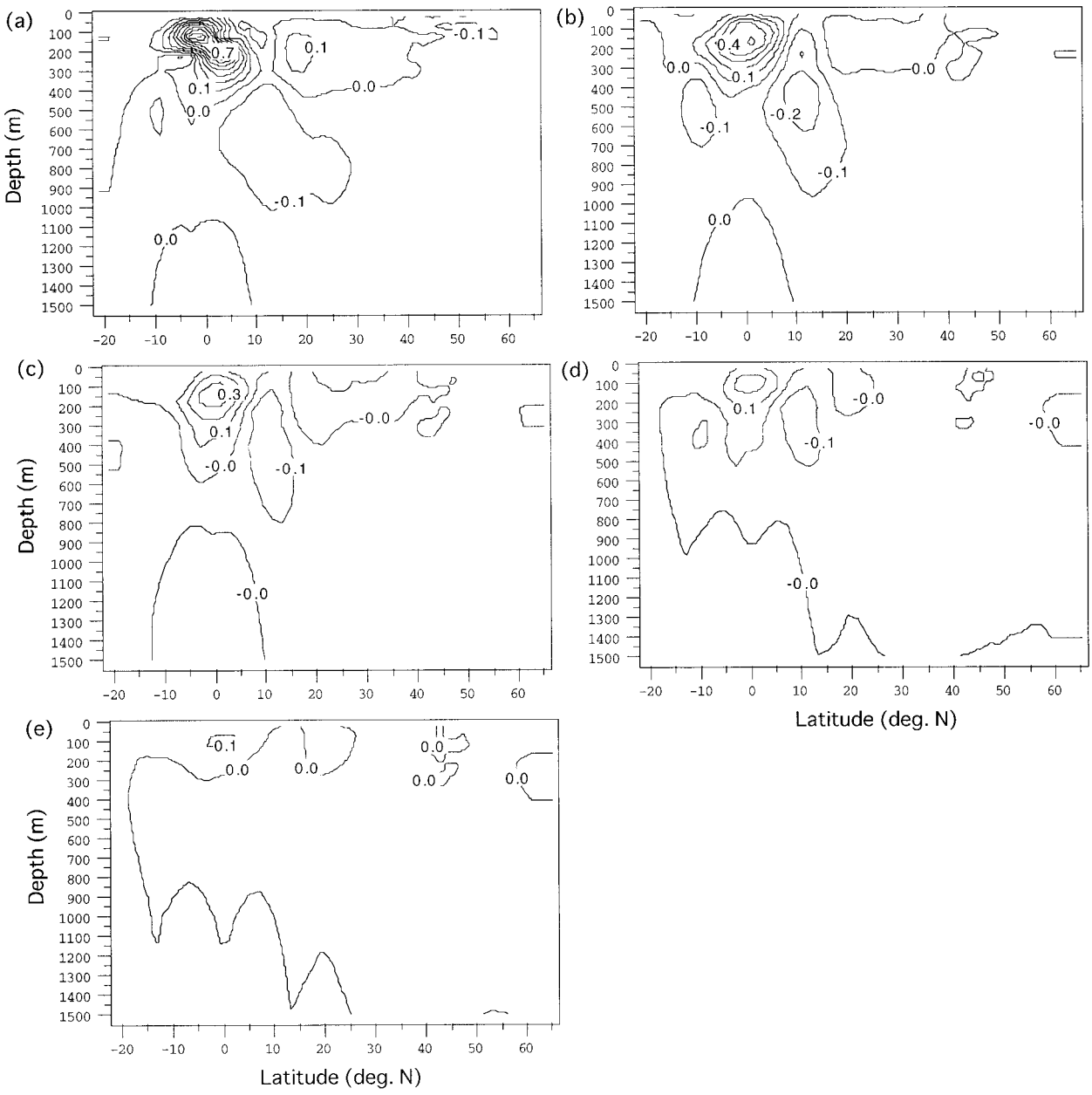

FIG. 3. Differences of zonally averaged Mar mean temperature of GMn − GMS for five different ratios (α) of tracer time step to velocity time step: (a) $\alpha = 48$, (b) $\alpha = 24$, (c) $\alpha = 12$, (d) $\alpha = 6$, and (e) $\alpha = 3$. Contour intervals are 0.1°C.

Probably the main reason is due to the destruction of geostrophic balance at the equator. We see from Fig. 5 that when α decreases from 48 to 12, the large difference in the western Tropics disappears. Presumably the thermocline depth is affected by the flow fields. The α value determines how close the case is to synchronous adjustment. In order to further understand the reason of the difference in trace distributions from different α values, we calculate the 20°C isotherm depth along the equator (actually at 1°N). The results from three different α values are shown in Fig. 6. At the area east of 240°E (120°W), there are two main differences between the asynchronous and synchronous integrations. One is the stronger upwelling taking place in summer in the synchronous integration. The other is that the horizontal gradient between 100- and 60-m contours is large in summer and autumn in the synchronous integration, while it is small in the asynchronous integration of large α (Fig. 6a). The results (not shown) from $\alpha = 3$ are almost the same as the synchronous ones except for small differences near the east boundary. The differences are probably caused by the different wave propagation from east to west due to different α values. At the most areas west of 240°E, the distribution patterns

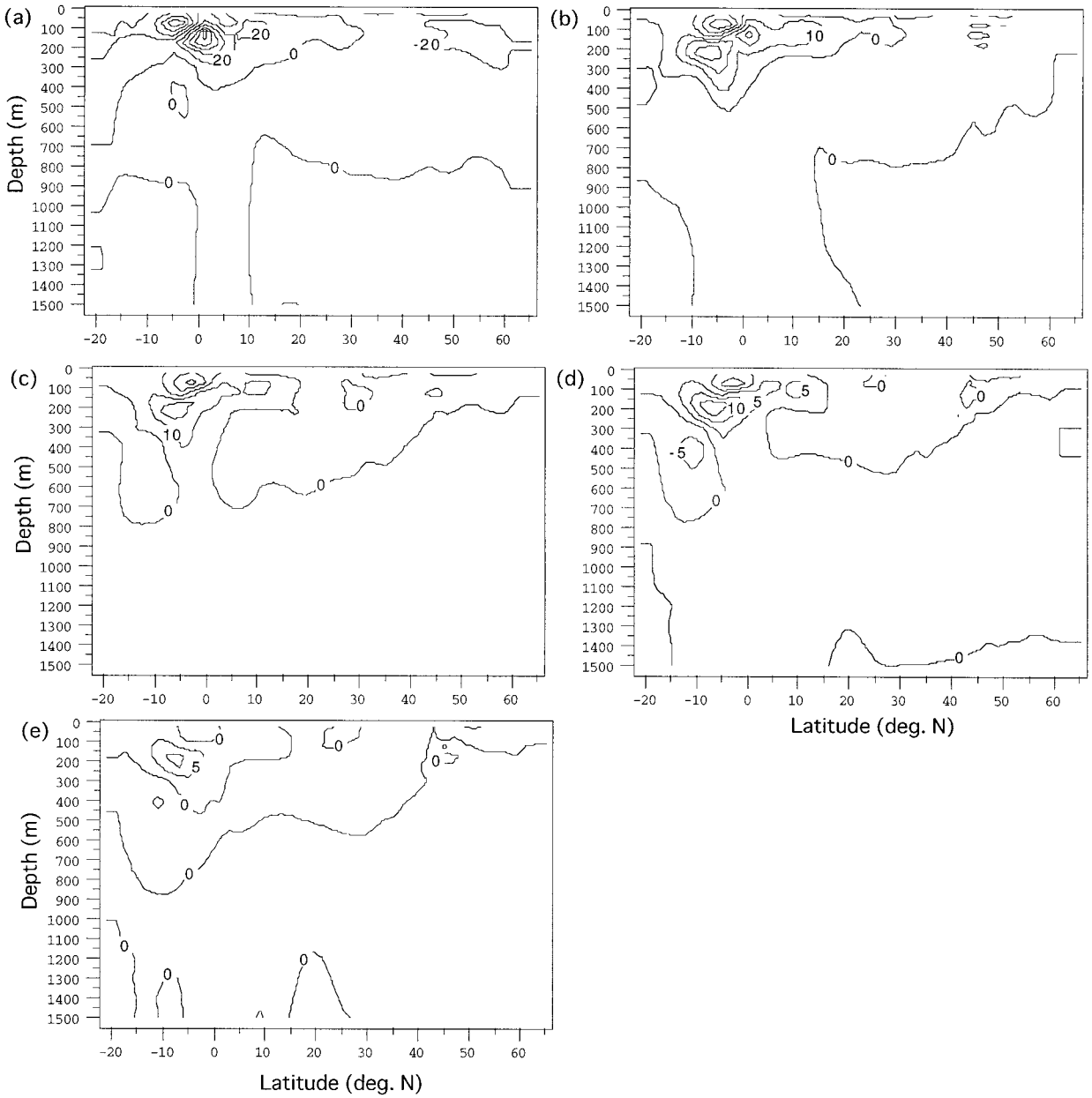

FIG. 4. As in Fig. 3 but for salinity. Contour intervals are (a) 20 (10^{-3}), (b) and (c) 10 (10^{-3}), and (e) and (f) 5 (10^{-3}).

of 20°C isotherm depth is quite similar between the synchronous and asynchronous integrations.

The above discussion is only concerned with active tracers, that is, temperature and salinity that affect circulation fields. Passive tracers (or anthropogenic tracers) do not affect the circulation field. In this study, we take CFCs as a reference to compare the difference between the asynchronous and synchronous integrations. Figure 7 shows the zonally averaged CFC-11 concentration distribution in March from the last year of 10 yr of integration using the GMS case, and the differences of CFC-11 concentrations between GMn ($n = 1, 3$) and GMS. Overall, the difference between asynchronous and synchronous integrations is not very large. For the largest value of $\alpha = 48$ (GM1), the accelerated integration overestimates CFC-11 penetrations by over 10% at the subsurface of the southern Tropics, and by about 5% at the subsurface of higher latitudes, compared with those from GMS. If α is reduced to 12, the difference is considerably reduced. We see that the difference at the subsurface of the southern Tropics is only about 3% in Fig. 7c while in higher latitudes it becomes less than 1%. When α is equal to 6, the difference in high latitudes almost disappears. The difference at the subsurface of the Tropics becomes much smaller, at about 2%. These differences are much smaller than the departure of cur-

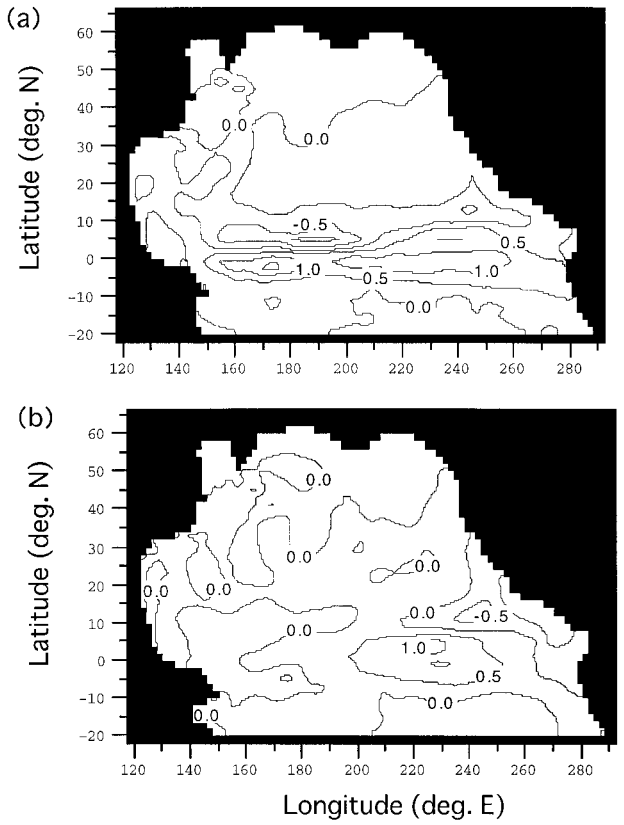

FIG. 5. Horizontal distributions of Mar mean temperature differences of (a) GM1 − GMS and (b) GM3 − GMS at the depth of 125 m. Contour intervals are 0.5°C.

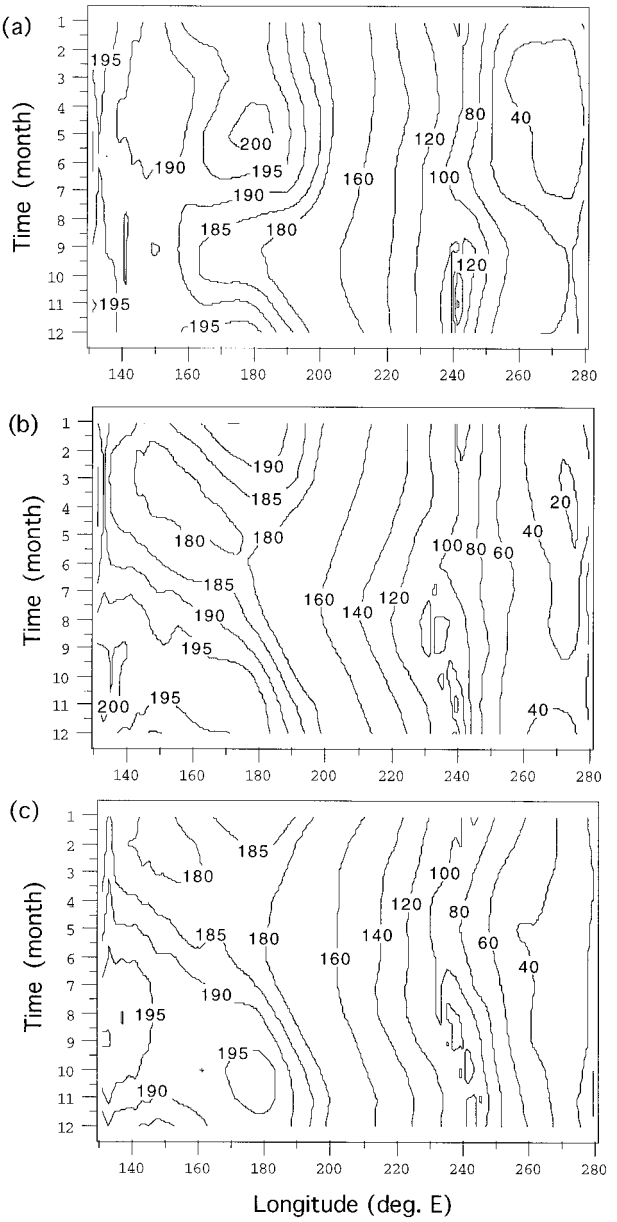

FIG. 6. Time–longitude sections of 20°C isotherm depth (m) along 1°N from different α values of (a) 48, (b) 12, and (c) 1.

rent model from the observations (Craig et al. 1998; Xu et al. 1999).

The difference between active and passive tracers is obvious. For passive tracers, the difference due to accelerated integration consists of two sources including dynamics and air–sea exchange. The dynamics is mainly due to transports. Different α values generate some different flow fields. Air–sea exchange fluxes of CFCs largely depend on temperature and salinity because both transfer velocity and solubility of CFCs are functions of temperature and salinity. Figure 8 shows a comparison of exchange fluxes from different α values. Figure 8a shows that the largest flux appears to be at about 42°N, 150°E, where surface temperature is low and wind speeds are high. The difference of fluxes is expressed as GMn (n = 1, 3, 4)-GMS in Figs. 8b–d. There are two main areas where accelerated integration generates some differences of fluxes relative to synchronous integration, including the western North Pacific (around 45°N, 160°E) and eastern tropical region. For the largest α value of 48, the difference in the western region is over 20%. The difference in the eastern tropical region can be as much as 50%. When the α value is reduced from 48 to 12, the difference due to accelerated integration is reduced considerably. In the western region, the difference is about 5%. The position of generating errors in the tropical region slightly moves toward the west. Both error and error coverage are considerably reduced. The improvement from α = 12 to α = 6 is not very apparent (Figs. 8c and 8d). Fluxes are more sensitive to α values than distributions are. These simple experiments confirm that when α is less than 12, the asynchronous integration of CFC model does not generate a significant error relative to the synchronous integration.

We have pointed out above the difference between active and passive tracers. We know from Fig. 7 that there is an obvious difference in CFC-11 distribution in

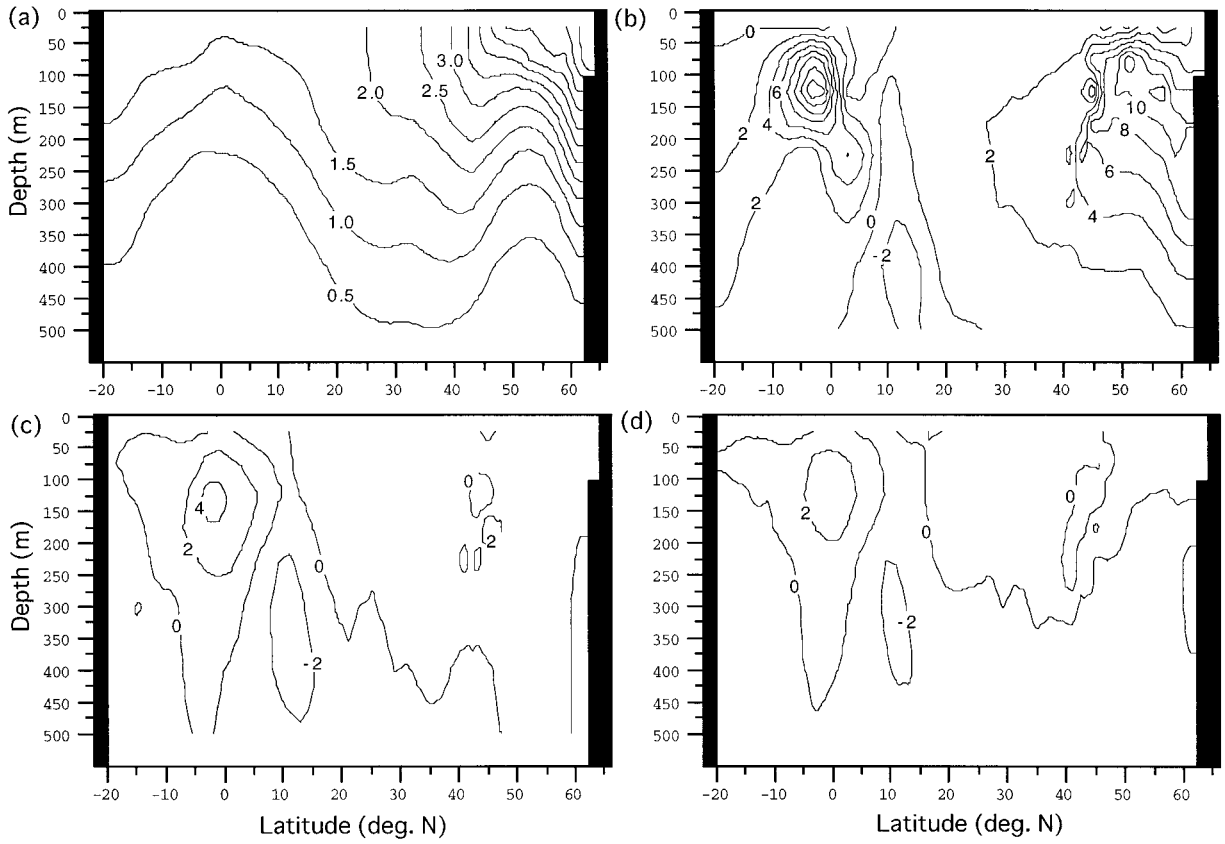

FIG. 7. Distributions of (a) zonally averaged Mar mean CFC-11 from GMS, and the CFC-11 differences of (b) GM1 − GMS, (c) GM3 − GMS, and (d) GM4 − GMS. Contour intervals are (a) 0.5 pmol kg^{-1} and (b), (c), (d) 2 (10^{-2}) pmol kg^{-1}.

higher latitudes between the asynchronous and synchronous integrations. However, we cannot see large differences in temperature and salinity in higher latitudes in both Figs. 3 and 4. CFC-11 has the large surface concentrations at the cold area in higher latitudes. A small difference in temperature and salinity can cause some differences at that area. Transports also contribute to the difference.

CFCs have a relatively short timescale for air–sea exchange in the mixed layer. This timescale is characteristic for nonreactive gases. In our model, the timescale for CFC-11 is about 15–35 days using a transfer velocity flux parameterization. Thus, surface concentrations display obvious seasonal variations. On the other hand, surface concentrations have spatial dependence because CFC-11 is sensitive to temperature. Comparing with CFCs, other reactive gases such as anthropogenic CO_2 have a relatively long timescale of air–sea exchange. Surface anthropogenic CO_2 does not have large seasonal variations. We found that there is a 5% difference in anthropogenic CO_2 at the subsurface of tropical region in March 1990 between $\alpha = 48$ and $\alpha = 6$. However, the difference in distributions of anthropogenic CO_2 is only about 1% between $\alpha = 12$ and $\alpha = 6$. The model for anthropogenic CO_2 can be found in Xu et al. (2000). As we have already known from the discussion of temperature and CFC-11, the difference of simulated results between $\alpha = 6$ and $\alpha = 1$ is very small. This indicates that the difference of anthropogenic CO_2 between the asynchronous and synchronous integrations is probably smaller than that found for CFC-11. The results from CFCs and anthropogenic CO_2 show that when α is less than 12, the asynchronous integration of passive tracer models does not yield a significant error relative to the synchronous integration. A similar conclusion can be made for other passive tracers.

4. Concluding remarks

In this paper we mainly discuss the differences of tracer distributions between asynchronous and synchronous integrations, and attempt to find out a suitable value of the ratio (α) of tracer time step to momentum time step in order to save computer time, but not to significantly affect the results. We have only examined tracer accelerations but not deep ocean accelerations. Several numerical experiments were conducted. Results show that a 15-yr integration adjustment is necessary for tracers to reach a new state at which there is a 1% difference relative to the final state upon a switch to a smaller trace time step from an equilibrium state. A large

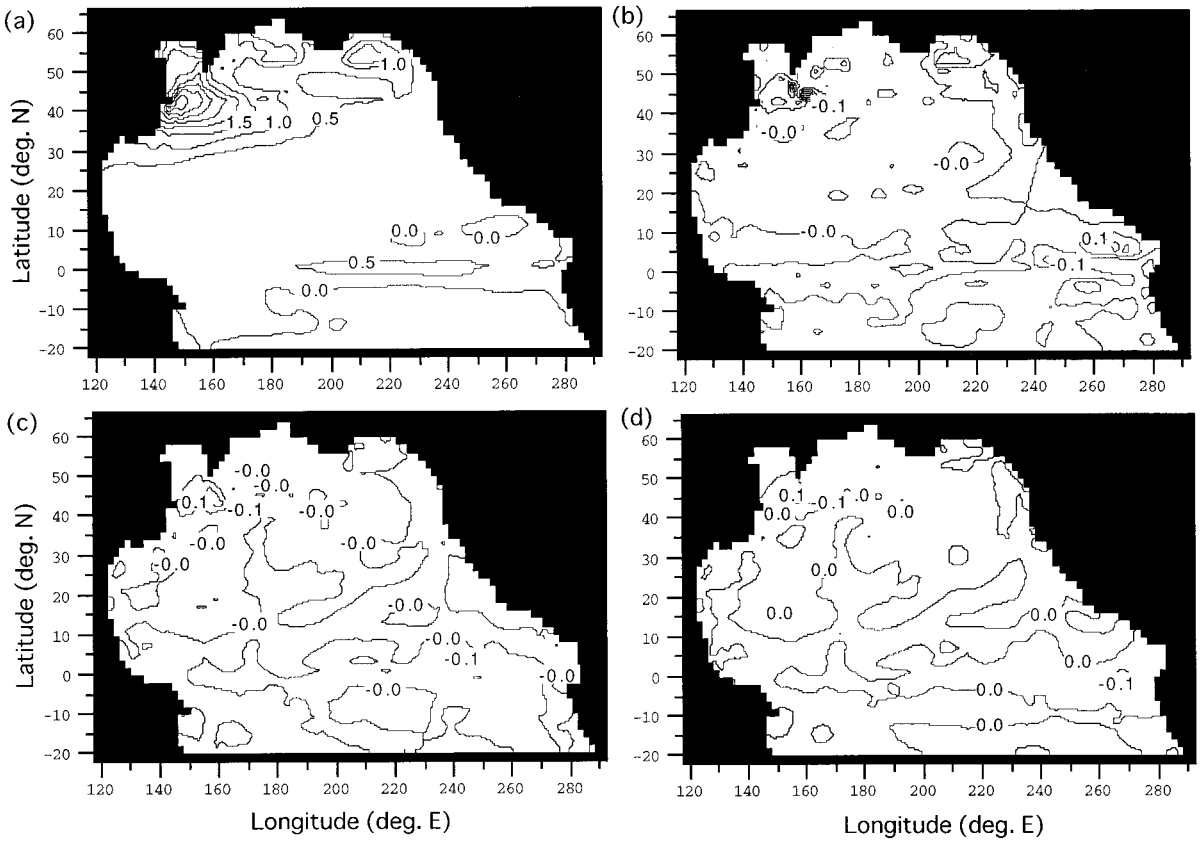

FIG. 8. Surface exchange fluxes (a) of CFC-11 in Mar 1989 from GMS and the flux differences of (b) GM1 − GMS, (c) GM3 − GMS, and (d) GM4 − GMS. Contour intervals are (a) 0.5×10^{-6} pmol cm^{-2} s^{-1} and (b), (c), (d) 0.1×10^{-6} pmol cm^{-2} s^{-1}.

value of 48 for α generally produces too large a departure from the synchronous integration. We estimate that if α is less than 6, the difference due to asynchronous integration is really negligible. If we allow a difference of 3% relative to synchronous integration, we can use the value of about 8 for α.

After we carefully examined active tracers of temperature and salinity, we have studied passive or anthropogenic tracers of CFCs. We mainly discussed the results of CFC-11. Results show that the largest α value of 48 generates an about 10% error in CFC-11 distributions at the subsurface of the southern Tropics and an about 5% error at the subsurface in higher latitudes, compared with those from GMS. Reducing α values can reduce the difference. We also mentioned the results of anthropogenic CO_2 that has a relatively long timescale of air–sea exchange. CFC errors due to accelerated integration are larger than those of active tracers and anthropogenic CO_2. The error for passive tracers is due to dynamics and air–sea exchange. If passive tracers are sensitive to temperature and salinity, they tend to produce a larger error, such as CFCs.

Acknowledgments. This study was supported by New Energy and Industrial Technology Development Organization (NEDO) as part of the ''Study of Environmental Assessment for Carbon Dioxide Ocean Sequestration for Mitigation of Climate Change (SEA-COSMIC).''

REFERENCES

Bryan, K., 1969: A numerical method for the study of the circulation of the world ocean. *J. Comput. Phys.,* **4,** 347–376.

——, 1984: Accelerating the convergence to equilibrium of ocean–climate models. *J. Phys. Oceanogr.,* **14,** 666–673.

——, and L. J. Lewis, 1979: A water mass model of the world ocean. *J. Geophys. Res.,* **84,** 2503–2517.

Bullister, J. L., and R. F. Weiss, 1988: Determination of CCl_3F and CCl_2F_2 in seawater and air. *Deep-Sea Res.,* **35A,** 839–853.

Craig, A. P., J. L. Bullister, D. E. Harrison, R. M. Chervin, and A. J. Semtner Jr., 1998: A comparison of temperature, salinity, and chlorofluorocarbon observations with results from a 1° resolution three-dimensional global ocean model. *J. Geophys. Res.,* **103** (C1), 1099–1119.

Danabasoglu, G., J. C. McWilliams, and W. G. Large, 1996: Approach to equilibrium in accelerated global oceanic models. *J. Climate,* **9,** 1092–1110.

Duffy, P. B., K. Caldeira, J. Selvaggi, and M. I. Hoffert, 1997: Effects of subgrid-scale mixing parameterizations on simulated distributions of natural ^{14}C, temperature, and salinity in a three-dimensional ocean general circulation model. *J. Phys. Oceanogr.,* **27,** 498–523.

Elkins, J. W., T. M. Thompson, T. H. Swanson, J. H. Butler, B. D. Hall, S. O. Cummings, D. A. Fisher, and A. G. Raffo, 1993: Decrease in the growth rates of atmospheric chlorofluorocarbons 11 and 12. *Nature,* **364,** 780–783.

England, M. H., and A. C. Hirst, 1997: Chlorofluorocarbon uptake in a world ocean model. 2. Sensitivity to surface thermohaline forcing and subsurface mixing parameterizations. *J. Geophys. Res.,* **102** (C7), 15 709–15 731.

Esbensen, S. K., and Y. Kushnir, 1981: The heat budget of the global ocean: An atlas based on estimate from surface marine observations. Rep. 29, Climate Research Institute, Oregon State University, Corvallis, OR, 27 pp.

Follows, M. J., and J. C. Marshall, 1996: On models of bomb ^{14}C in the North Atlantic. *J. Geophys. Res.,* **101** (C10), 22 577–22 582.

Gent, P. R., and J. C. McWilliams, 1990: Isopycnal mixing in ocean circulation models. *J. Phys. Oceanogr.,* **20,** 150–155.

——, J. Willebrand, T. J. McDougall, and J. C. McWilliams, 1995: Parameterizing eddy-induced tracer transports in ocean circulation models. *J. Phys. Oceanogr.,* **25,** 463–474.

Hellerman, S., and M. Rosenstein, 1983: Normal monthly wind stress over the world ocean with error estimates. *J. Phys. Oceanogr.,* **13,** 1093–1104.

Ishida, A., K. Nakata, S. Aoki, H. Kutsukake, M. Kishi, and M. Kubota, 1995: Numerical experiment of anthropogenic CO_2 in the North Pacific. *J. Adv. Mar. Sci. Technol. Soc.,* **1,** 49–62.

Levitus, S., and T. P. Boyer, 1994: *Temperature.* Vol. 4, *World Ocean Atlas 1994,* NOAA Atlas NESDIS 4, 117 pp.

——, R. Burgett, and T. P. Boyer, 1994: *Salinity.* Vol. 3, *World Ocean Atlas 1994,* NOAA Atlas NESDIS 3, 99 pp.

Sarmiento, J. L., 1986: On the North and tropical Atlantic heat balance. *J. Geophys. Res.,* **91,** 11 677–11 689.

Wanninkhof, R., 1992: Relationship between wind speed and gas exchange over the ocean. *J. Geophys. Res.,* **97,** 7373–7382.

Warner, M. J., and R. F. Weiss, 1985: Solubilities of chlorofluorocarbons 11 and 12 in water and seawater. *Deep-Sea Res.,* **32,** 1485–1497.

Weaver, A. J., and E. S. Sarachik, 1991: The role of mixed boundary conditions in numerical models of the ocean's climate. *J. Phys. Oceanogr.,* **21,** 1470–1493.

Xu, Y., K. Nakata, A. Ishida, S. Aoki, and K. Harada, 1999: Simulations of chlorofluorocarbon uptake in a model of the North Pacific. *J. Adv. Mar. Sci. Technol. Soc.,* **5,** 1–18.

——, Y. W. Watanabe, S. Aoki, and K. Harada, 2000: Simulations of storage of anthropogenic CO_2 in the North Pacific using an ocean general circulation model. *Mar. Chem.,* **72,** 221–238.